# RESEARCH ON THE EFFECT OF MICRO AND MACRO SYNTHETIC FIBRE ON PLASTIC SHRINKAGE CRACKING OF CONCRETE

## Based on the Shrinkage Ring Test as set out in ÖVBB Guideline 2008

Tested fibre types and dosages:

fibrillated micro fibre – 1 kg/m$^3$

monofilament micro fibre – 1 kg/m$^3$

BarChip MQ58 synthetic macro fibre – 1, 1.5 and 2 kg/m$^3$

Dr. Peter K. Juhasz

Peter Schaul

September, 2021

JKP Static Ltd.
FEA • concrete engineering • material test
+36 (70) 330-9149 • +36 (1) 239-9368 • office@jkp.hu • www.jkpstatic.com

# Table of contents

**1. Preliminaries** ..... 3
**2. Test specimens** ..... 3
**3. Testing procedure** ..... 7
**4. Expression of results** ..... 11
**4.1. Measuring crack length** ..... 11
**4.2. Measuring crack width** ..... 11
**4.3. Measuring and calculating crack surface** ..... 12
**4.4. Maximum and average crack width definition** ..... 12
**4.5. Efficiencies** ..... 13
**5. Results** ..... 13
**5.1. Total crack length** ..... 13
**5.2. Maximum and average crack width** ..... 14
**5.3. Total crack surface** ..... 14
**5.4. Efficiencies** ..... 15
**6. Summary** ..... 16
**7. Conclusion** ..... 17
**8. References** ..... 17
**9. Appendix – Photos of the cracked rings** ..... 18

## 1. Preliminaries

Plastic shrinkage behaviour of plain and fibre reinforced concrete was investigated based on the Shrinkage Ring Test as set out in Österreichische Vereinigung für Beton und Bautechnik Guideline (ÖVBB, 2008). The tests were carried out at JKP Static Concrete Laboratory, Budapest.

## 2. Test specimens

The measurements are performed on concrete rings with a width of 150 mm and a depth of 40 mm. The concrete specimens are cast in a mould consisting of two concentric steel rings fixed on a rigid plywood panel (Figure 1). Inside the outer ring of the mould 12 steel sheets are placed to constrain the concrete and to initiate cracking.

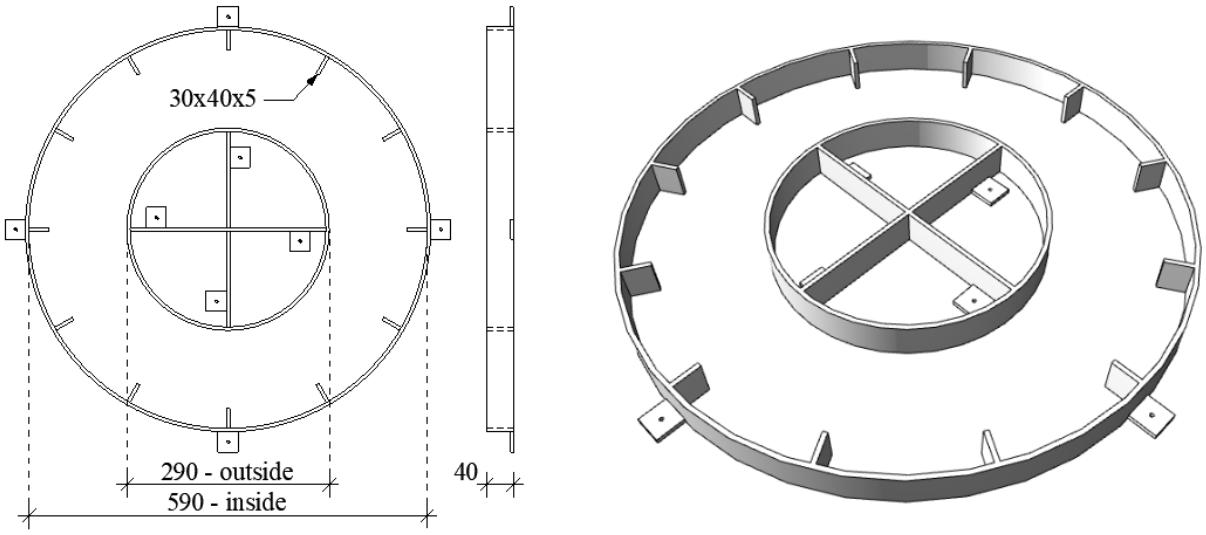


**Figure 1.** Steel mould for shrinkage test

Two types of concrete were investigated made from two types of cement: CEM III/A 32.5 N cement and CEM I 52.5 R cement. These two types of cement were selected to cover different concrete types. This is well reflected in the research: the different concretes had a significantly different crack propagation. The concrete mix, using 500 kg/m$^3$ fines (the minimum required by ÖVBB), can be seen in Table 1.

**Table 1.** Concrete mix proportions

| Component | Type | [kg/m$^3$] |
|---|---|---|
| Cement | CEM III/A 32.5 N and CEM I 52.5 R | 360 |
| Water content | | 220 |
| Limestone powder | | 130 |
| Aggregate 0/4 | | 447 |
| Aggregate 4/8 | | 757 |
| Aggregate 8/16 | | 395 |
| w/c | 0.61 | |

The concrete mix design follows the recommendation of ÖVBB, which is not a typical flooring mix design, but used to demonstrate the effect of fibres on early age crack development. The concrete strength class was C20/25 for both concrete types, due to its high water/cement ratio (see Table 2). The slump of the plain concrete was 220 mm, no superplasticiser was added.

**Table 2.** Compressive strength of plain concrete

| Specimen | *a* [mm] | *b* [mm] | Force [kN] | Strength [MPa] | mean/standard deviation |
|---|---|---|---|---|---|
| CEM III/1 | 150 | 150 | 670 | 29.80 | $f_{cm,test}$ = 31.7<br>$s_n$ = 2.27 |
| CEM III/2 | 150 | 150 | 685 | 30.46 | |
| CEM III/3 | 150 | 150 | 786 | 34.93 | |
| CEM I/1 | 150 | 150 | 780 | 34.74 | $f_{cm,test}$ = 34.4<br>$s_n$ = 4.32 |
| CEM I/2 | 150 | 150 | 888 | 39.49 | |
| CEM I/3 | 150 | 150 | 650 | 28.91 | |

The types of fibre reinforcement can be seen in Table 3 and in Figure 2, and the dosages can be seen in Table 3.

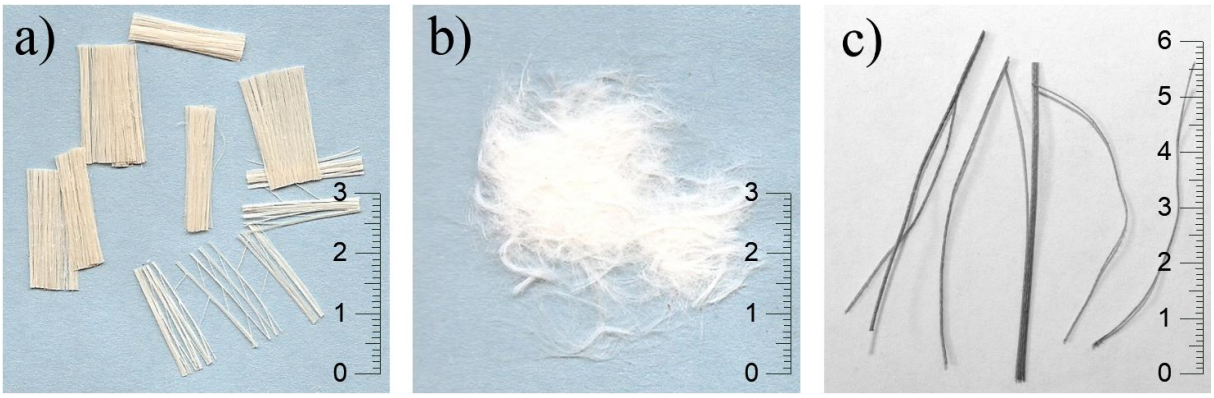


**Figure 2.** a) fibrillated b) monofilament c) BarChip MQ58

**Table 3.** Fibre properties (data provided by manufacturer)

| | |
|---|---|
| **Fibrillated (HG)** | |
| Base resin | Polyolefin |
| Specific gravity | 0.91 g/cm$^3$ |
| Form | Micro fibrillated |
| Length | 19 mm |
| Equivalent diameter | N/A |
| Tensile strength | 400 MPa |
| Young's modulus | 4.9 GPa |
| Melting point | 150 °C |
| **Monofilament (MU)** | |
| Base resin | Polyolefin |
| Specific gravity | 0.91 g/cm$^3$ |
| Form | Micro monofilament |
| Length | 12.7 mm |
| Equivalent diameter | 32 μm |
| Tensile strength | 270 MPa |
| Young's modulus | N/A |
| Melting point | 160 °C |
| **MQ58 – BarChip (MQ)** | |
| Base resin | Bi-Component Polymer |
| Specific gravity | 0.90 – 0.92 g/cm$^3$ |
| Form | Macro, surface embossed |
| Length | 58 mm |
| Equivalent diameter | 670 μm |
| Tensile strength | 640 MPa |
| Young's modulus | 10 GPa |
| Melting point | 120 – 170 °C |

Three specimens were prepared for each parameter variation according to Table 4, one ring each per casting date. CEM III: 15/3/2021; 18/3/2021 (two sets cast on the same day); CEM I: 19/3/2021; 22/3/2021 (two sets cast on the same day).

**Table 4.** Research matrix

| Ring name | Cement type | Fibre type – fibre dosage |
|---|---|---|
| PC-CEMIII-date | CEM III/A 32.5 N | - |
| HG-CEMIII-date | CEM III/A 32.5 N | fibrillated – 1 kg/m$^3$ |
| MU-CEMIII-date | CEM III/A 32.5 N | monofilament – 1 kg/m$^3$ |
| MQ10-CEMIII-date | CEM III/A 32.5 N | MQ58 – 1 kg/m$^3$ |
| MQ15-CEMIII-date | CEM III/A 32.5 N | MQ58 – 1.5 kg/m$^3$ |
| MQ20-CEMIII-date | CEM III/A 32.5 N | MQ58 – 2 kg/m$^3$ |
| PC-CEMI-date | CEM I 52.5 R | - |
| HG-CEMI-date | CEM I 52.5 R | fibrillated – 1 kg/m$^3$ |
| MU-CEMI-date | CEM I 52.5 R | monofilament – 1 kg/m$^3$ |
| MQ10-CEMI-date | CEM I 52.5 R | MQ58 – 1 kg/m$^3$ |
| MQ15-CEMI-date | CEM I 52.5 R | MQ58 – 1.5 kg/m$^3$ |
| MQ20-CEMI-date | CEM I 52.5 R | MQ58 – 2 kg/m$^3$ |

After installation of the steel ring on the plywood table the surface of the plywood table and the inner steel ring were coated with form oil (Figure 3). Figure 4 and 5 show the filling procedure of the moulds.

**Figure 3.** Mould coated with form oil

**Figure 4.** Filling of the mould

**Figure 5.** Filling of the mould

Concrete was compacted by tamping and the surface finished with a wooden float to achieve a smooth finish so that any cracks were easily visible.

## 3. Testing procedure

Testing started immediately after finishing the specimens. The air above the specimens was agitated by a fan (minimum capacity of 490 $m^3$/h) surrounded by a crescent air funnel placed over the concrete rings and generating a minimum wind speed of 4 m/s over the concrete surface (Figure 6).


**Figure 6.** Measuring the wind speed with an anemometer

Two specimens were tested per tunnel setup (Figure 9). A modified approach was adopted which followed the process implemented by Fenyvesi (2012), where a foil tent was placed over all of the rings, which were tested simultaneously. It is expected this modification provides similar conditions to the ÖVBB requirements. The duration of the measurements was 5 hours at 20 °C (± 2 °C) and 50% (± 5%) relative humidity (Figure 8). In previous research conducted by the authors using the same methodology it was observed that in all cases, if a crack had not formed after 5 hours it would not form even if the test was extended until 8 hours (as suggested by the OVBB recommendation). Hence, once the 5 hour mark was reached, the test was stopped. The temperature and humidity was monitored during this time at half hour intervals (Figure 7). To maintain the desired values a mobile climate machine was used in the closed laboratory. After the end of the test, the lengths of all observed cracks in each specimen were accumulated and the total crack lengths of the FRC and control plain concrete were compared.

However, the length of the cracks is not a decisive measurement, as typically more cracks will result in smaller crack widths which are less critical in practice.

The order of the rings were different on each day to eliminate the effect of the distance from the fan. The order of the rings per test are in Table 5.

The concrete mixtures for all types of concretes were prepared before the concreting to minimise the time difference between the first and last rings. The time difference was about 15 minutes. The crack measurement started after the 5 hours elapsed.

The laboratory humidity was initially lower than 50%, however as the concrete began to hydrate, and water evaporated from the surface during the drying period, the humidity increased and was then able to be maintained at 50% for the duration of the test.

**Table 5.** Order of the rings per date

| | | | |
|---|---|---|---|
| Test 1 | FAN1 | PC | HG |
| | FAN2 | MU | MQ10 |
| | FAN3 | MQ15 | MQ20 |
| Test 2 | FAN1 | MQ10 | MU |
| | FAN2 | MQ20 | MQ15 |
| | FAN3 | HG | PC |
| Test 3 | FAN1 | MQ15 | MQ20 |
| | FAN2 | PC | HG |
| | FAN3 | MU | MQ10 |

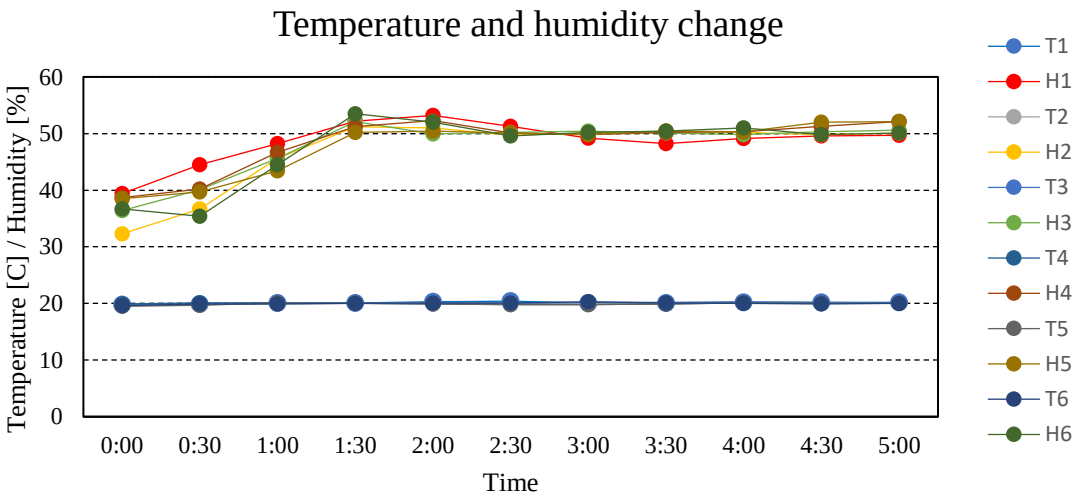


**Figure 7.** Temperature and humidity change as a function of time for all six testing periods

**Figure 8.** Installation of the moulds and the fan

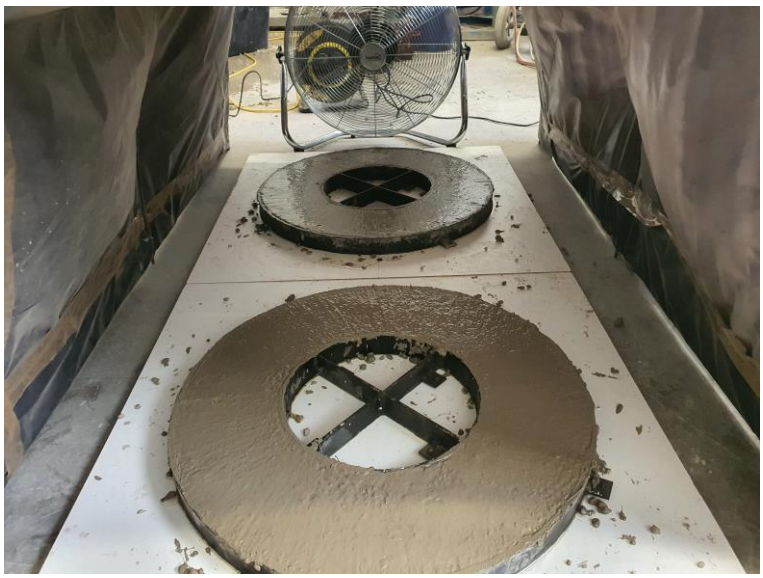

**Figure 9.** Moulds in the tent


**Figure 10.** Measuring of the temperature and humidity in the tent during the test (the climate control device was inside of the testing tunnel, and taken out for photograph)

## 4. Expression of results

### 4.1. Measuring crack length

The crack is a visible separation of the concrete on the top surface of the ring. The length of a single crack was measured according to Figure 11. by means of a ruler.

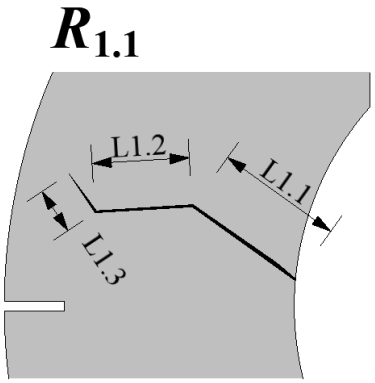


**Figure 11.** Length of a single crack, $L_{R1.1} = \Sigma L_{1.i}$

The total length of a series ($L_{total}$) is the sum of the single cracks on the same types of specimens (same concrete, fibre type and dosage), according to Figure 12.

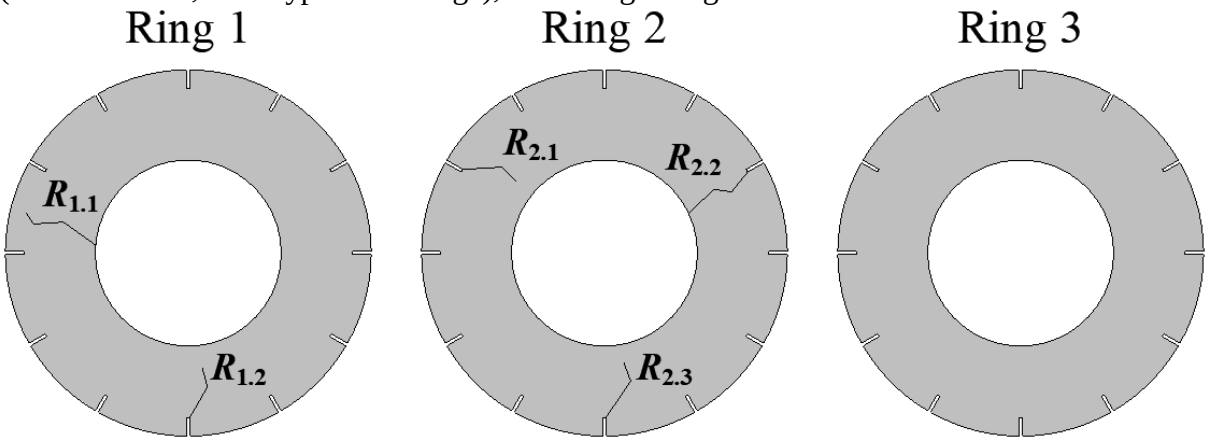


**Figure 12.** Total length of a series, $L_{total} = \Sigma L_{Ri.j}$

### 4.2. Measuring crack width

The crack width was measured with a crack width ruler. The crack was measured at every 40 mm on the length of the crack, according to Figure 13.

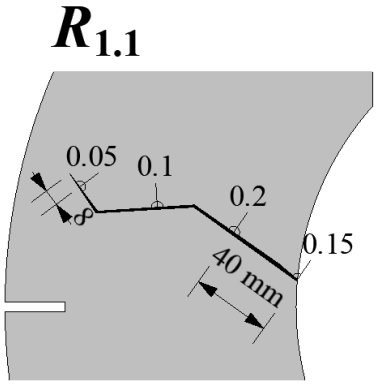


**Figure 13.** Measuring the crack width on a single crack

The maximum crack width of a single crack is the maximum value along the crack length. The maximum crack width ($w_{max}$) of a series is the maximum crack width of all the cracks in the series.

### 4.3. Measuring and calculating crack surface

Crack surface is an integration of the crack width along the crack length. The calculating method is numerical integration, the method is shown by an example in Figure 13 and Table 6.

**Table 6.** Crack surface calculation of single crack R1.1 according to Figure 13.

| $l$ = segment length [mm] | $a$ = crack width start [mm] | $b$ = crack width end [mm] | $M = (a+b)/2$ mean crack width [mm] | $A = M \times l$ crack surface [mm$^2$] |
|---|---|---|---|---|
| 40 | 0.15 | 0.20 | 0.175 | 7.0 |
| 40 | 0.20 | 0.10 | 0.15 | 6.0 |
| 40 | 0.10 | 0.05 | 0.075 | 3.0 |
| 8 | 0.05 | 0.00 | 0.025 | 0.2 |
| Crack surface of single crack R1.1 | | | | **16.2** |

Total crack surface is the sum of crack surfaces of single cracks in a series:

$$A_{\text{total}} = \sum_{\text{i=1}}^{\text{n}} A_i \qquad (1)$$

where $A_{total}$ is the total crack surface of a series, $n$ is the number of cracks in the series, $A_i$ is the crack surface of single crack $i$.

### 4.4. Maximum and average crack width definition

Maximum crack width ($w_{max}$) of a series is according to 5.2. The mean crack width ($w_{mean}$) is according to the following equation:

$$w_{\text{mean}} = \frac{A_{\text{total}}}{L_{\text{total}}} \tag{2}$$

### 4.5. Efficiencies

The crack widths, lengths and crack surfaces were measured after the end of the test, according to previous Chapters 5.1-4. From these data two efficiencies were calculated; efficiency of reduction of crack surface ($\eta_a$), and efficiency of reduction of maximum crack width ($\eta_w$) with the following equations:

$$\eta_a = \frac{A_{\text{total,plain}} - A_{\text{total,FRC}}}{A_{\text{total,plain}}} \times 100 \tag{3}$$

$$\eta_w = \frac{w_{\text{max,plain}} - w_{\text{max,FRC}}}{w_{\text{max,plain}}} \times 100 \tag{4}$$

## 5. Results

### 5.1. Total crack length

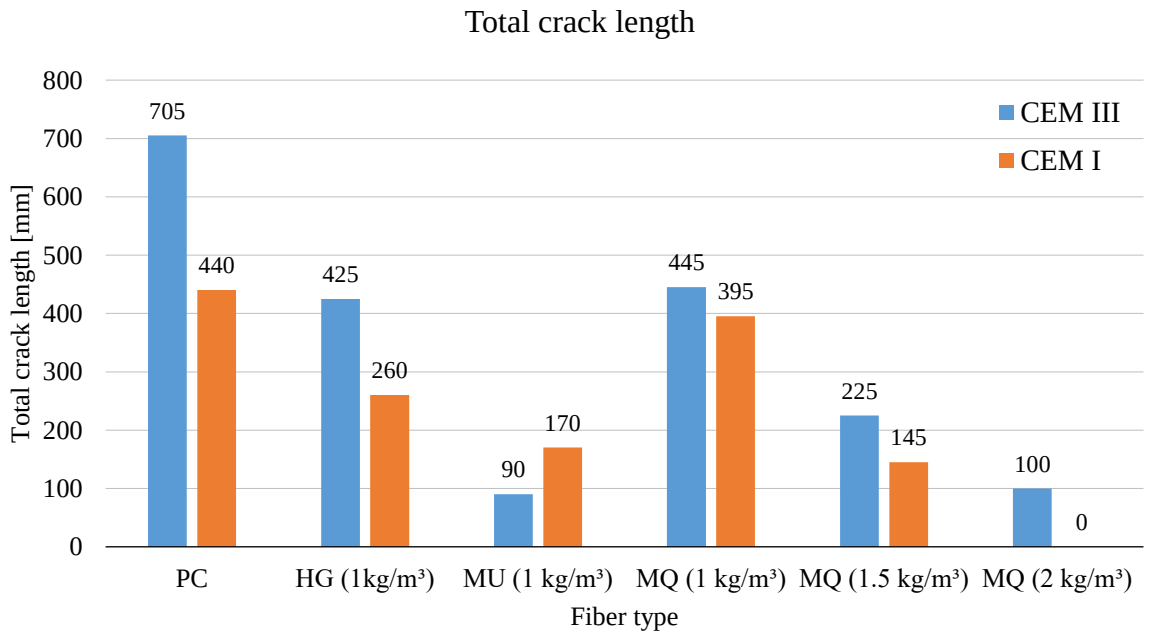


**Figure 14.** Total crack length

## 5.2. Maximum and average crack width

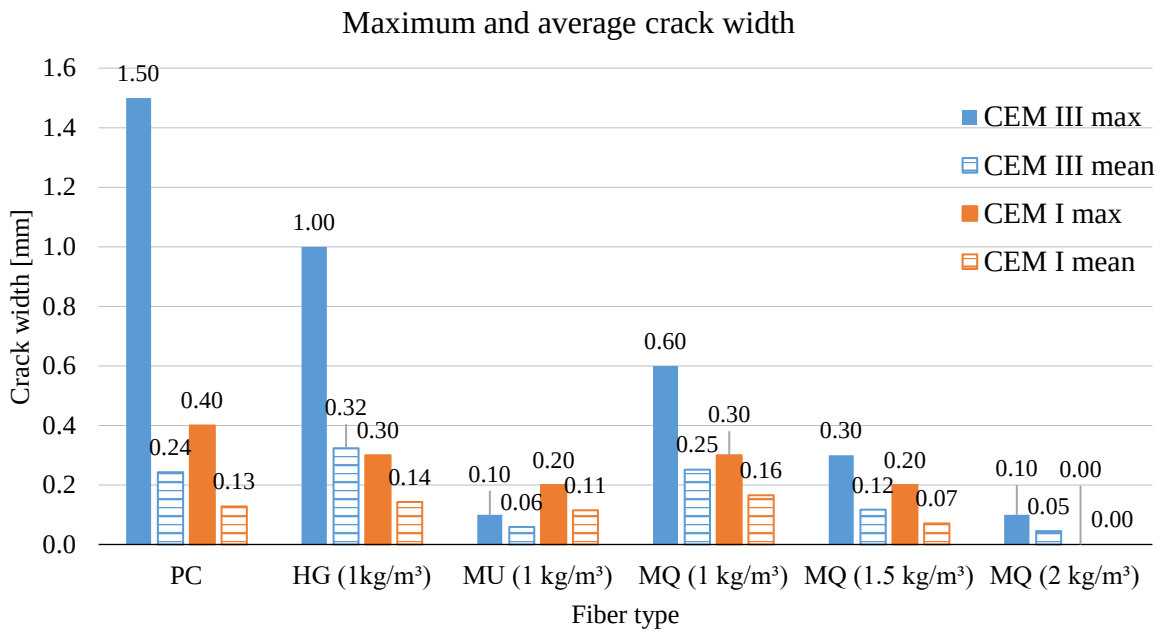


**Figure 15.** Maximum and average crack width

## 5.3. Total crack surface

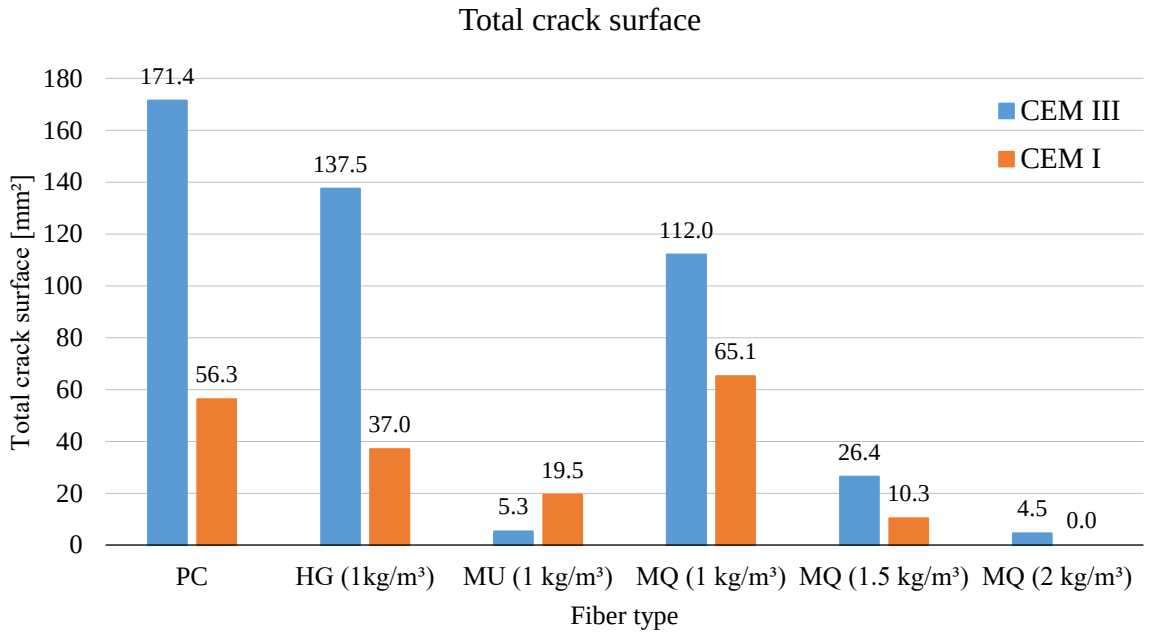


**Figure 16.** Total crack surfaces

It is assumed that the reduced total crack surface of the CEM I series compared to the CEM III types is due to its higher early strength development.

## 5.4. Efficiencies

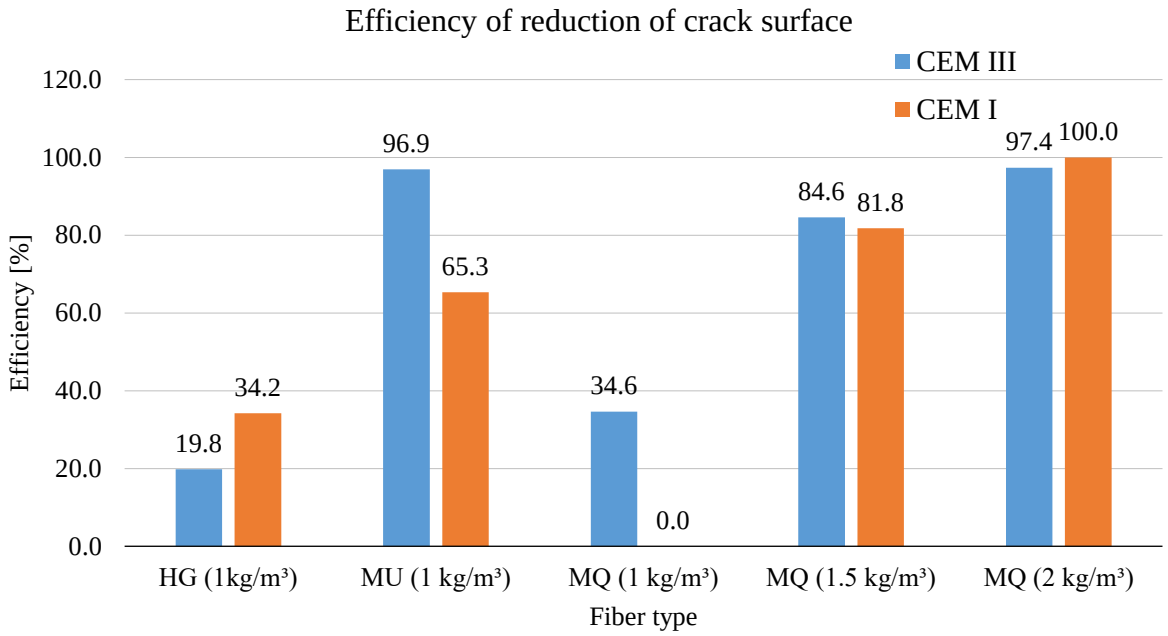


**Figure 17.** Efficiency of reduction of crack surface

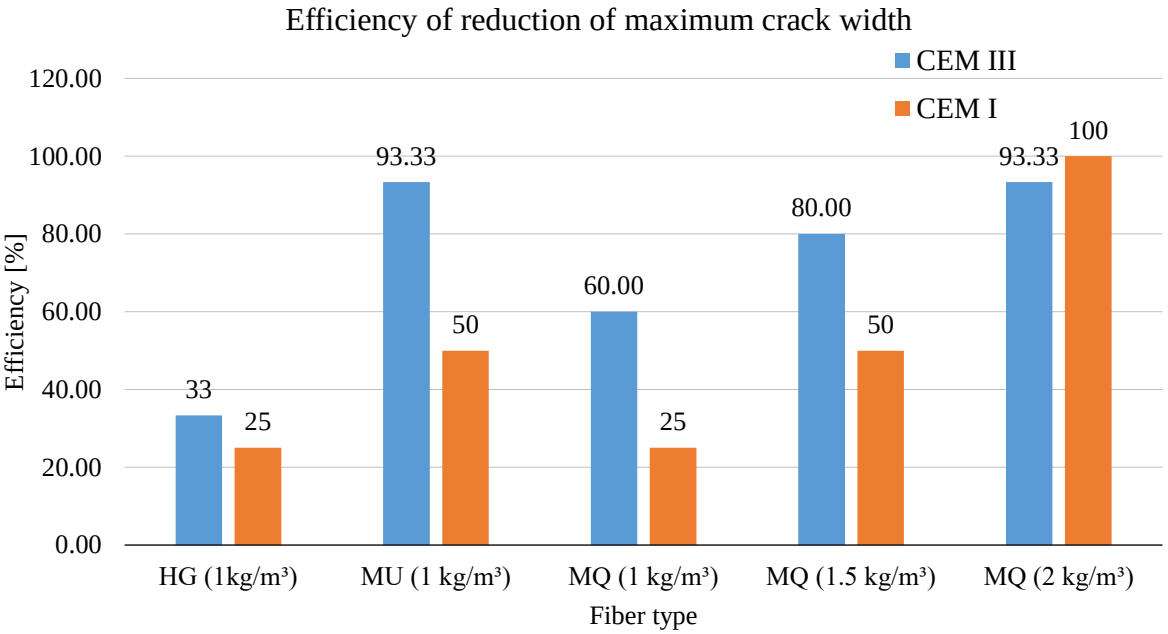


**Figure 18.** Efficiency of reduction of maximum crack width

## 6. Summary

In this research, the impact of macro synthetic fibres on the early age shrinkage crack propagation of concrete was assessed while being compared and contrasted with two commercially available micro synthetic fibres that are promoted for their ability to reduce early age plastic shrinkage cracking. Macro synthetic fibres are generally only acknowledged and used for their enhanced post-cracking strength, however this research has demonstrated that certain macro synthetic fibres can also assist in reducing the propensity for early age (plastic) shrinkage cracking in concrete.

The research followed the guidance provided in the ÖVBB Richtlinie Faserbeton with with some practical changes adopted, such as the use of the wind tunnels to effect the drying of the concrete surfaces as proposed by Fenyvesi.

Measurements of crack length were made, as requested in the ÖVBB guideline, while crack widths were also measured by the authors, in order to derive the crack surface area, a measurement that the authors feel provides a more complete overview of the impact of fibres on the early age crack development. For each of the three outcomes it was clearly seen that for each fibre, except the monofilament PP fibres, that the crack development in the CEM III rings was more pronounced than the cracking in the CEM I rings. For the monofilament PP fibres, the CEM I rings had greater cracking than the CEM III rings. It is proposed that for the majority of results that the earlier strength development of the CEM I concrete reduced the propensity for early age shrinkage cracks to develop, however that does not explain why the monofilament PP fibre concretes behaved differently. It was not the purpose of this research to determine the impact of different cements, rather the effect of various fibres.

Each measured outcome (crack length, width & surface area) followed a similar trend. Summarising the CEM III results, the plain concrete showed the most severe cracking, while the fibrillated micro PP and monofilament PP fibres reduced the crack surface area by 19.8% and 96.9% respectively. It can clearly be seen here that the monofilament PP fibres are far more effective than fibrillated PP fibres. Interestingly, the macro synthetic fibres also demonstrated a significant reduction in the early age crack propagation compared to the plain concrete. The macro synthetic fibres were used at dose rates of 1.0, 1.5 and 2.0 kg/m$^3$ with crack surface area being reduced by 34.6, 84.6 and 97.4% respectively, compared to plain concrete. Hence, the 1.0 kg dose rate provided similar behaviour to the fibrillated PP fibres, while dose rates of 1.5 and 2.0 kg/m$^3$ displayed similar reductions to the monofilament PP fibres, which are well known for their ability to reduce early age shrinkage cracks. It can also be seen that the macro synthetic fibres provide a significant improvement over the fibrillated PP fibres in terms of reducing the early age crack surface area. The dose rates of 1.0, 1.5 and 2.0 kg/m$^3$ provided reductions of 18.6, 80.8 and 96.8% compared to the fibrillated PP fibres.

The exploitation of the average crack widths yields some remarkable effects. Firstly, the absolute numbers of average crack widths tend to be generally lower for the CEM I concrete types as compared to the CEM III types. The reason is expected to be in the quicker hydration development and crystallisation process as mentioned before.

A similar performance of the different fibres can be observed however. The fibrillated micro fibre shows no beneficial effect at all as compared to the plain concrete types. Within the CEM III types the monofilament micro fibre shows a 75% reduction, while there is only 15% in the CEM I group.

The macro synthetic fibre (BarChip MQ58) shows a remarkable 50% reduction versus the plain concretes at a dose rate of 1.5 kg/m$^3$. At the higher dose rate of 2.0 kg/m$^3$ a 79% reduction can be noted in CEM III, while a total reduction of average crack width can be observed in the CEM I types.

## 7. Conclusion

From this research it becomes clear that certain macro synthetic fibres (BarChip MQ58) can provide equal or better behaviour, in terms of early age shrinkage crack development, than commercially available fibrillated and monofilament micro PP fibres at dose rates of 1.0, 1.5 and 2.0 kg/m$^3$.

## 8. References

Österreichische Vereinigung für Beton- und Bautechnik (2008). *Richtlinie Faserbeton*, Vienna, Austria.

Fenyvesi, O. (2012). *Early age shrinkage cracking tendency of concretes*, PhD thesis, Budapest University of Technology and Economics.

## 9. Appendix – Photos of the cracked rings


**PC-CEMIII-20210315**


**HG-CEMIII-20210315**


**MU-CEMIII-20210315**


**MQ10-CEMIII-20210315**


**MQ15-CEMIII-20210315**


**MQ20-CEMIII-20210315**


**PC-CEMIII-20210318AM**


**HG-CEMIII-20210318AM**

**MU-CEMIII-20210318AM**


**MQ10-CEMIII-20210318AM**

**MQ15-CEMIII-20210318AM**

**MQ20-CEMIII-20210318AM**


**PC-CEMIII-20210318PM**

**HG-CEMIII-20210318PM**

**MU-CEMIII-20210318PM**


**MQ10-CEMIII-20210318PM**

**MQ15-CEMIII-20210318PM**

**MQ20-CEMIII-20210318PM**


**PC-CEMI-20210319**


**HG-CEMI-20210319**


**MU-CEMI-20210319**


**MQ10-CEMI-20210319**


**MQ15-CEMI-20210319**

**MQ20-CEMI-20210319**


**PC-CEMI-20210322AM**


**HG-CEMI-20210322AM**


**MU-CEMI-20210322AM**


**MQ10-CEMI-20210322AM**

**MQ15-CEMI-20210322AM**

**MQ20-CEMI-20210322AM**


**PC-CEMI-20210322PM**

**HG-CEMI-20210322PM**

**MU-CEMI-20210322PM**

**MQ10-CEMI-20210322PM**

**MQ15-CEMI-20210322PM**

**MQ20-CEMI-20210322PM**